END TO END PROCESS SIMULATION OF THE HIGH PRESSURE RESIN TRANSFER MOLDING PROCESS

Nathan Sharp, Johnathan Goodsell, Byron Pipes
Composites Manufacturing and Simulation Center, Purdue University

Abstract

An end-to-end process simulation has been created to predict the high pressure resin transfer molding (HP-RTM) process. Material properties such as fiber orientations and resin properties are mapped throughout the process so that a performance model can be run on a part as it is actually manufactured, not just as it is designed. A B-Pillar geometry was used as a demonstration part and showed a difference in residual deformation of almost 20% when the as-manufactured material properties were considered.

Introduction

While carbon fiber reinforced polymers (CFRPs) are often considered materials, in actuality they are structures. The fiber architecture within a CFRP is largely what determines its properties. Because there are too many fibers to model explicitly, homogenization techniques are used to get properties of the CFRP treating it as if it were a homogeneous material. These techniques work well as long as the assumed microstructure that is used to homogenize is accurate. However, if the microstructure is significantly different from the assumed microstructure, the estimated laminate properties can have large errors[1]. This can be problematic for designers of CFRP parts because many manufacturing processes cause the microstructure to change. If these changes are not taken into account, designers may be designing based on properties which can in actuality never be achieved in a real part because the assumed microstructure cannot realistically be made. In order for a performance model to have accurate predictions, an end-to-end manufacturing process model must first be run so that the performance analysis considers the as-manufactured part, properties and state. This is called “manufacturing-informed performance simulation.”

The HP-RTM manufacturing process includes 6 main steps, shown below in figure 1. The starting point is a roll of carbon or glass fiber fabric. The next step is to cut the fabric into the flat shapes necessary to make the desired part geometry. The cut fabric is stacked and assembled into a fiber mat and placed into a two-sided mold. The mold is then compressed so the fiber mat conforms to the desired geometry. At this point resin is infused at high temperatures and pressures so that it infuses through the preform very quickly. The mold remains at high pressures and temperatures for a time to allow the resin to completely cure, at which point the mold is opened and the part is cooled and removed. The physical phenomena associated with the last four process steps as well as their influence on the design process are outlined in figure 2.

Figure 1: HP-RTM process flow diagram.

PREFORMING	RESIN INFUSION	HEATED CURE	DEMOLDING
Fabric shearing and deformation Determines tow/fiber orientation Affects modulus, strength, warpage	**Darcy Flow** Determines impregnation Affects consolidation and warpage	**Cure Kinetics** Determines polymer properties Affects internal stresses and warpage	**Residual Stresses & Deformations** Determines final part shape Affects strength and tolerances
Tooling-preform interaction can cause excessive shearing & wrinkling	Improper gating/venting/pressure can cause incomplete fill or washout	Incomplete cure reduces polymer properties	Improper tooling can yield out-of-tolerance geometric deviations

Figure 2: Physical phenomena associated with HP-RTM process steps.

Virtual Manufacturing Process

The manufacturing process steps outlined previously are simulated with analogous virtual steps. The draping step is modeled in order to predict the fiber directions and shearing strains that result from draping a fabric over a complex geometry. Since composite material properties are dominated by fiber direction, this result will affect all subsequent steps. The infusion and cure steps are modeled together because the physics behind the two steps are coupled together with infusion speeds being a function of degree of cure and both steps being a function of temperature, which is often not isothermal for HP-RTM. The demolding step will import fiber direction,

temperature, and curing behavior to aid in the prediction of the part warpage and residual stress state. All of the manufacturing effects are then brought into the performance model so that the effective properties, residual stress state, and final shape of the manufactured part can all be included into the performance analysis. Figure 3 shows a flow diagram of the virtual manufacturing process described above.

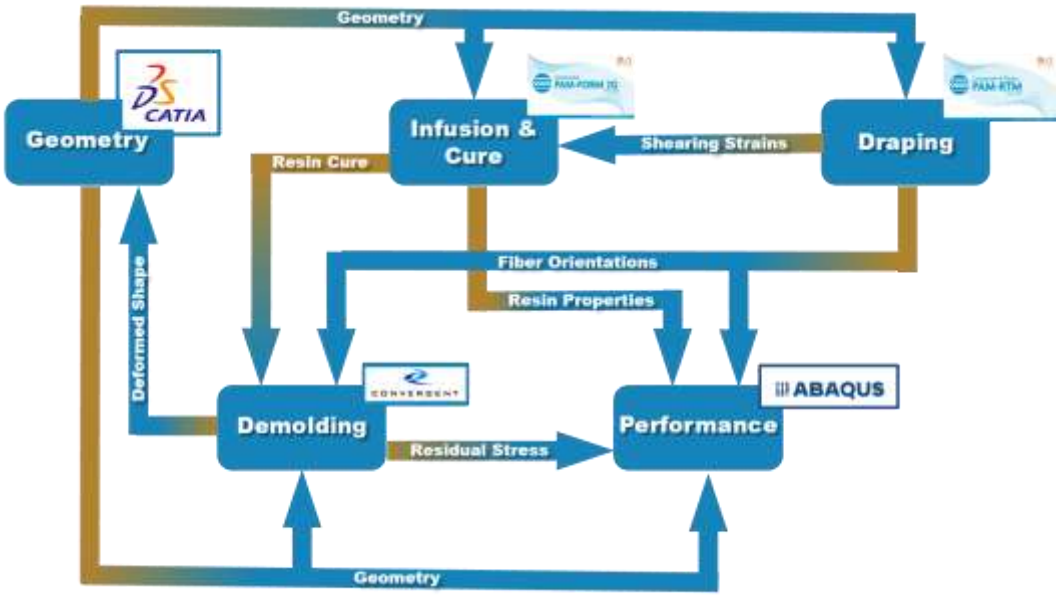

Figure 3: Virtual manufacturing flow diagram.

Demonstration Part Geometry

In order to demonstrate the virtual manufacturing process, a part must be selected to perform the process on. An automotive B-Pillar was selected as the demonstration part, shown in figure 3. A Hexcel IM7 carbon twill fabric was selected with the properties as shown in table 1. The part consists of 4 plies of the twill fabric. The fabric is laid down with a 0/90 fabric followed by two ±45 layers of fabric and another 0/90 fabric on top. The 0 degree direction is along the x direction as shown in Figure 4.

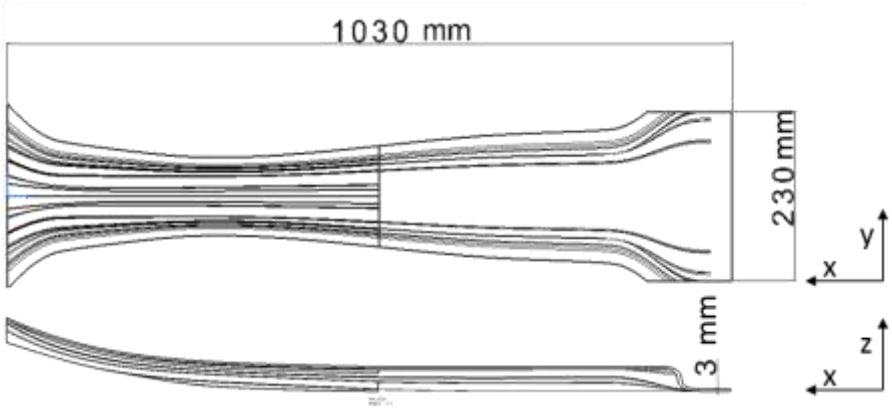

Figure 4: B-Pillar part dimensions.

Table 1: Carbon twill fabric properties.

Parameter	**Value**
Fiber modulus (GPa)	276
Bending stiffnes (N/mm)	60
Aerial weight (g/m^2)	300
Permeability (m^2)	1e-11

Physical Phenomena

The physics behind all of the HP-RTM steps identified in figure 2 are well known and can be modeled using commercially available software packages. We will briefly discuss the physics behind each virtual step; a more complete description of the modeling techniques of each step can be found in documentation of the software packages used in each virtual step.

Draping

Since composite fabrics experience a large rigid body rotation and small strain during draping process, the analysis of draping process is typically a geometrically nonlinear problem. By ignoring the body force, the variational weak form of the governing equation can be expressed in the reference configuration by[2]:

$$\int_{\Omega} \rho \ddot{u}_i \delta u_i \mathrm{d}\Omega + \int_{\Omega} S_{ij}\, \delta E_{ij} \mathrm{d}\Omega - \int_{\Gamma} t_i \delta u_i \mathrm{d}\Gamma = 0 \quad , \tag{1}$$

where Ω and Γ are the volume of the undeformed fabric and the boundary surface of the deformed fabric, respectively; ρ is the mass density; u_i designates the vector of displacement and rotation; $\ddot{u}_i$ represents the acceleration; t_i is the surface traction vector initially applied on Γ; S_{ij} and E_{ij} are respectively the second Piola-Kirchhoff stress tensor (PK2) and Green-Lagrange strain tensor which are given by:

$$S_{ij} = J \frac{\partial X_i}{\partial x_k} \frac{\partial X_j}{\partial x_m} \sigma_{km,} \tag{2}$$

$$E_{ij} = \frac{1}{2}\left(\frac{\partial u_i}{\partial X_j} + \frac{\partial u_j}{\partial X_i} + \frac{\partial u_k}{\partial X_i}\frac{\partial u_k}{\partial X_j}\right), \tag{3}$$

where X_i and x_k are the components of the positions vector of a point of the membrane in the undeformed configuration and deformed configuration, respectively; J is the Jacobian determinant which is given by $J = \det F$ with F being deformation gradient.

Infusion and Cure

While infusion and cure steps were separated above, they will be included together in the virtual steps because they are coupled with cure rate being a function of temperature and viscosity being a function of both temperature and degree of cure. All modeling of resin will use Hexcel RTM6 resin material properties.

Cure Kinetics

While resin is being infused through the fabric it is also curing. The cure kinetics of Hexcel RTM6 resin has been reported previously in the literature[3] by Panagiotis et al. and the cure kinetics model reported by them is also used in this simulation:

$$\frac{d\alpha}{dt} = (k_1 + k_2\alpha^m)(1-\alpha)^n, \tag{4}$$

where ki is defined as:

$$k_i = A_i exp\left(\frac{-E_i}{RT}\right), \tag{5}$$

with the model parameters as outlined in table 2.

Table 2: Cure kinetics model parameters.

Parameter	**A_1 (s^{-1})**	**E_1 (kJ/mol)**	**A_2 (s^{-1})**	**E_2(kJ/mol)**	**m**	**n**
Value	20340	70.2	6656	53.2	1.28	1.51

Infusion Modeling (Darcy's Law)

Darcy's Law states that the velocity of a fluid through a porous media is a function of the pressure gradient, viscosity of the fluid, and permeability of the porous media:

$$\nabla P = \frac{\eta}{\bar{K}}\boldsymbol{v}, \tag{6}$$

where v is the velocity vector, P the pressure, η the viscosity, and K the permeability tensor. In this equation the viscosity and permeability are material input parameters and the pressure and velocities are unknowns. The continuity equation is also needed to fully constrain the problem:

$$\frac{\partial\rho}{\partial t} + \nabla\cdot\rho v = 0, \tag{7}$$

where t is time and ρ is density. In-plane permeability of fabrics has been shown to be sensitive to shear strains[4], which is why the shear strains caused by draping are imported from the draping simulation and included in the simulation. The viscosity of the resin was modeled using the RTM6 viscosity model as reported by Kiuna et al[5]:

$$\frac{d\eta}{dt} = \eta\left[k(T) + \frac{1}{\eta_0}\frac{d\eta_0}{dt}\right], \tag{8}$$

where *k(T)* is defined as,

$$k(T) = A_2\exp\left(\frac{-E_2}{RT}\right), \tag{9}$$

and η_0 is defined as,

$$\eta_0(T) = A_1 \exp\left(\frac{E_1}{RT}\right). \quad (10)$$

Table 3 shows the parameters for the model described above.

Table 3: Viscosity model parameters.

Parameter	A_1 (Pa s)	E_1 (J/kg)	A_2 (s^{-1})	E_2(J/kg)
Value	$7.3x10^{-4}$	$1.3x10^{4}$	$7.4x10^{4}$	$6.5x10^{4}$

Deformation

Part deformation during demolding coming from the relieving of internal stresses which develop during the molding and cooldown process will be modeled using Convergent's commercial simulation package COMPRO. The governing equations for the stress/deformation that develops during the molding, cooldown, and demolding steps are[6-8]:

$$\Pi_P = U + \Omega, \quad (11)$$

$$\Pi_P = \int_V \frac{1}{2}\varepsilon^T D\varepsilon \, dV - \int_V \frac{1}{2}\varepsilon^T D\varepsilon_0 \, dV - \int_V \frac{1}{2}\varepsilon^T \sigma_0 \, dV - \int_V \frac{1}{2}u^T X \, dV - \int_S u_s^T q_s dS, \quad (12)$$

where U is internal work, Ω is external work, $\boldsymbol{\varepsilon}$ is the strain tensor, $\boldsymbol{\sigma}$ is the stress tensor, $\boldsymbol{\varepsilon_0}$ is free/thermal strain, $\boldsymbol{\sigma_0}$ is the initial stress tensor, u is the displacement vector, X is body forces, and q_s is surface forces. There are several phenomena contributing to stresses and deformations during an HP-RTM manufacturing process. Typically the largest contribution to internal stresses in a carbon-epoxy part is the mismatch in coefficients of thermal expansion between the carbon fiber and the resin[9]. However, cure shrinkage, cure and cure rate gradients, and tool-part interaction also contribute[10].

Results

The simulations outlined in section 4 were completed on the B-Pillar geometry outlined in figure 4 and connected as described in figure 3.

Draping Analysis

When a fabric is preformed into a tool shape, there are three main modes of fabric deformation. The dominant deformation mode is shearing of the fabric by tows sliding past each other, or, if shear locking angle has been reached, wrinkling out of the plane. Bending of the fabric out of the plane is also important for the fabric to conform to a complex geometry. The last possible deformation mode is from the tows in the fabric stretching axially; however, because the fibers are so stiff compared to the other two deformation modes, axial stretching is a secondary effect in draping analyses.

The fiber tow modulus was measured using a TA Q800 DMA. The bending stiffness was measured using a Taber fabric stiffness tester. Both values are listed in Table 1. The shearing behavior is measured using a picture frame test, so called because the test fixture looks like a picture frame. The results of the picture frame test are shown in figure 5. Picture frame test results are typically comprised of a relatively flat region followed by a sharp increase in the slope at a certain point. This point is called the shear lock angle and corresponds to the point where the tows can no longer slide past each other and additional shearing can only occur by tows buckling out of the plane. This is also the point where wrinkling occurs and in this fabric the data shows that the shear lock angle occurs at around a 25 degree shear angle. The force as a function of shear angle is input directly into PAM-FORM. Given these inputs PAM-FORM estimates the fabric behavior as it is pressed in the mold. Figure 6 shows the shear angle of the preform in both the 45 layers and the 0 layers. The estimates show a significant amount of shearing (but well below the shear lock angle) in both plies at either end of the part.

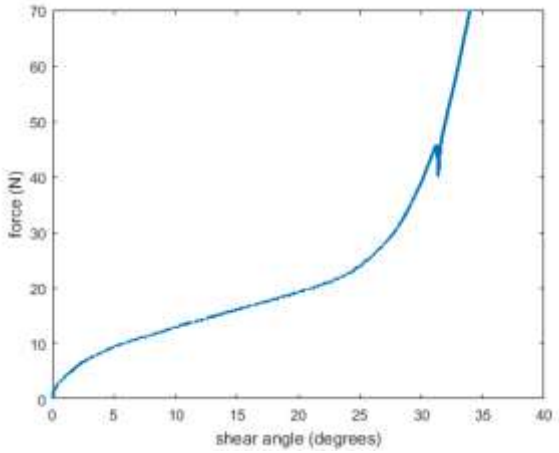

Figure 5: force as a function of shear angle of the carbon twill fabric.

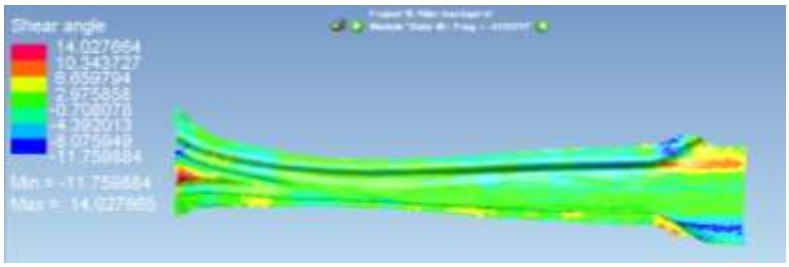

(a)

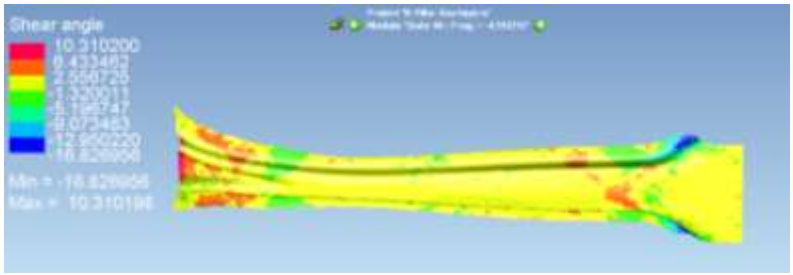

(b)

Figure 6: Shear angles for the pressed preform in the (a) top layer (0/90) and (b) second layer (45/-45).

Infusion and Cure Analysis

As previously mentioned, there are several things happening simultaneously during the infusion and cure step. Figure 7 outlines the state variables and dependencies of different physical phenomena that are occurring during this step.

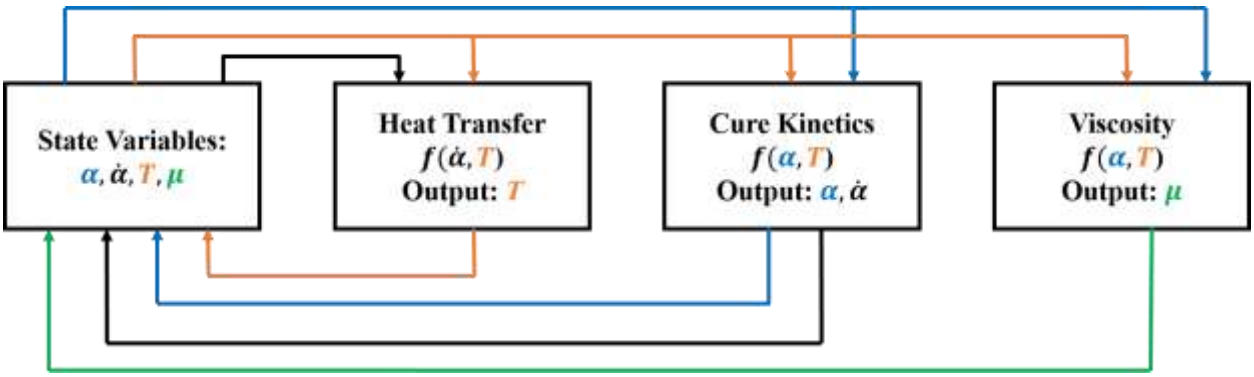

Figure 7: Flow of information during the infusion and cure step.

The permeability of the fabric is listed in table 1 and the effect of shear angle on permeability was estimated based on the literature[11]. The shear angle were imported directly from PAM-FORM into PAM-RTM. A gate was placed in the center of the part and vents were placed along the edges in the long direction. Figure 8 shows a contour plot of the resin fill time and resin cure state at complete fill. This information can be useful for several reasons. First, the model can be used to minimize the fill time by optimizing the gate and vent locations, especially in areas of high shear which will change the permeability behavior. Also, the resin cure state at the time in which the infusion is completed is useful in predicting the part deformation, residual stress, and material properties.

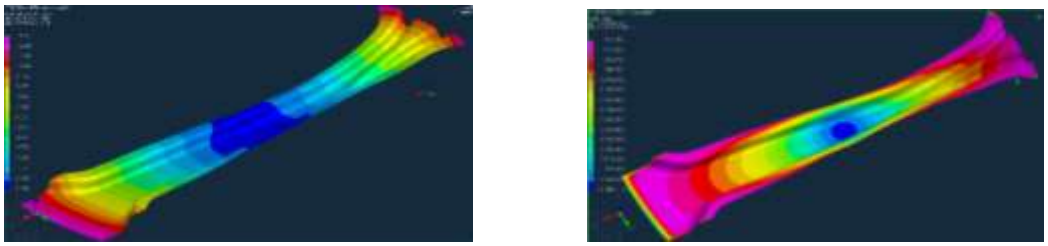

(a) (b)

Figure 8: (a) Resin fill time and (b) degree of cure at complete fill.

Deformation Analysis

The stress and deformation analysis starts with the part at complete fill and ends with the cooled, demolded part. The final deformed shape as well as the residual stress after deformation are both predicted. Cure shrinkage and coefficients of thermal expansion are the factors driving the stress and deformation[12-13]. The draped fiber orientations are imported from PAM-FORM and the resin cure states at complete fill are imported from PAM-RTM. During the molding step, the part was constrained to be attached to the mold through a surface contact constraint. At demolding the contact constraint was removed and the only boundary constraints applied were to prevent rigid body motion. Figure 9 shows the deformation and residual stress of the draped part. As a means of comparison, the simulation was also run with the as-designed fiber orientation and uniform initial cure state. The results of this analysis are shown in figure 10. The as-designed part underpredicted the maximum deformation as compared to the part which in included manufacturing effects by almost 20 percent, highlighting the significant impact the manufacturing effects can have on the part properties.

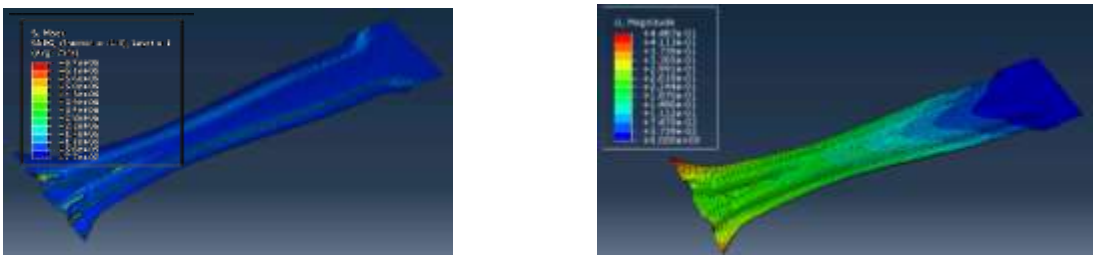

(a) (b)

Figure 9: (a) deformation magnitude and (b) residual stress in part with imported orientation.

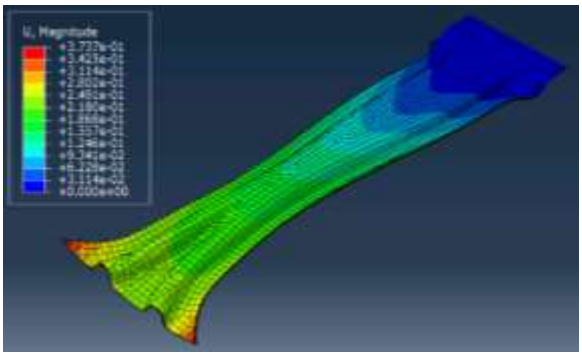

Figure 10: The as-designed part underpredicts deformation by almost 20 percent.

Tooling Geometry Compensation

If the deformation predicted by the COMPRO analysis is enough to make the part geometry outside of acceptable tolerance limits, then the tooling geometry can be compensated such that the part will deform into the desired shape[14-15]. This can be done by importing the deformation vectors from ABAQUS into CATIA using the Dassault product Composites Link and morphing the tool geometry by the deformation vectors but in the reverse direction. The process described above can be iterated until all analyses show satisfactory results. Figure 11 shows an example of the geometry compensation. Going through this end to end process simulation before beginning

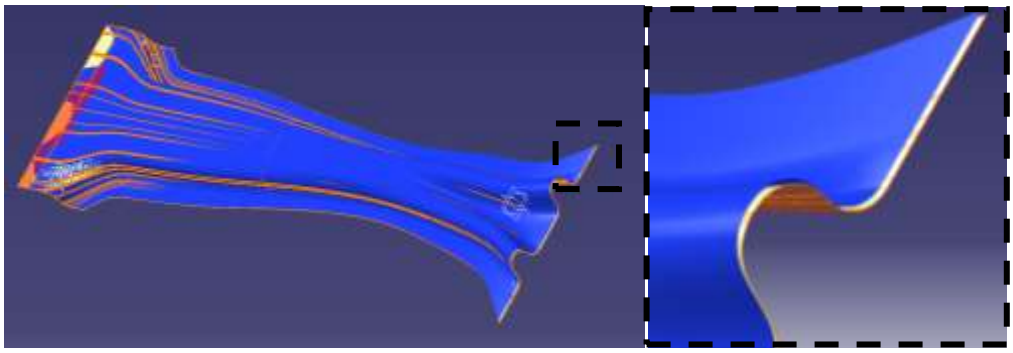

Figure 11: Geometry compensation using Composites Link and CATIA.

manufacturing or performance modeling provides several benefits: the process parameters such as gate and vent locations, pressure, and temperature can be optimized, the mold geometry can be made to account for process induced deformation, and the performance model can be made more accurate by modeling the as-manufactured part instead of the as-designed part.

Summary and Next Steps

We have presented an integrated process simulation for high-pressure resin transfer molding. The process integrates the commercial simulation tools CATIA, PAM-FORM, PAM-RTM, ABAQUS and COMPRO to provide an end-to-end process simulation for the HP-RTM process. An example of the process was shown for a generic b-pillar geometry to illustrate the physical phenomenon and the simulation tool connectivity. Of particular interest is the prediction of fabric shearing, resin flow front and the final residual stress state and deformations and the resulting as-manufactured part geometry. The use of the process simulation to predict the tooling compensation necessary to achieve the as-designed geometry was illustrated.

More generally, in a part with geometrical complexity, the manufacturing process will cause the as-manufactured microstructure to differ from the as-designed microstructure. Since the composite's properties are highly dependent on its microstructure, manufacturing can significantly affect the deformation of the part, its residual stress state and its strength and stiffness performance. While these phenomenon have been demonstrated for HP-RTM using an end-to-end process simulation, the implications of manufacturing-informed performance apply to composites manufacturing in general.

References

1. Hahn, Hong T., and Stephen W. Tsai. *Introduction to composite materials*. CRC Press, 1980.
2. Van Der Weeën, F. "Algorithms for draping fabrics on doubly-curved surfaces." *International journal for numerical methods in engineering* 31.7 (1991): 1415-1426.
3. Karkanas, Panagiotis I., and Ivana K. Partridge. "Cure modeling and monitoring of epoxy/amine resin systems. I. Cure kinetics modeling." *Journal of applied polymer science* 77.7 (2000): 1419-1431.
4. Heardman, E., C. Lekakou, and M. G. Bader. "In-plane permeability of sheared fabrics." *Composites Part A: Applied Science and Manufacturing* 32.7 (2001): 933-940.
5. Kiuna, N., et al. "A model for resin viscosity during cure in the resin transfer moulding process." *Composites Part A: Applied Science and Manufacturing* 33.11 (2002): 1497-1503.
6. A. Johnston. An integrated model of the development of process-induced deformation in autoclave processing of composite structures. PhD Thesis. The University of British Columbia, Vancouver, Canada (1997).

7. A. Johnston, R. Vaziri and A. Poursartip. A Plane Strain Model for Process-Induced Deformation of Laminated Composite Structures. Journal of Composite Materials 2001; 35(16):1435-1469.
8. Wang, Xiaojun, and D. D. L. Chung. "Residual stress in carbon fiber embedded in epoxy, studied by simultaneous measurement of applied stress and electrical resistance." *Composite Interfaces* 5.3 (1997): 277-281.
9. Parlevliet, Patricia P., Harald EN Bersee, and Adriaan Beukers. "Residual stresses in thermoplastic composites—A study of the literature—Part I: Formation of residual stresses." *Composites Part A: Applied Science and Manufacturing* 37.11 (2006): 1847-1857.
10. Jung, Woo-Kyun, et al. "Measurement and compensation of spring-back of a hybrid composite beam." *Journal of composite materials* 41.7 (2007): 851-864.
11. Castro, J. M., and C. W. Macosko. "Studies of mold filling and curing in the reaction injection molding process." *AIChE Journal* 28.2 (1982): 250-260.
12. Radford, Donald W. "Cure shrinkage induced warpage in flat uni-axial composites." *Journal of Composites, Technology and Research* 15.4 (1993): 290-296.
13. Parlevliet, Patricia P., Harald EN Bersee, and Adriaan Beukers. "Residual stresses in thermoplastic composites—A study of the literature—Part I: Formation of residual stresses." *Composites Part A: Applied Science and Manufacturing* 37.11 (2006): 1847-1857.
14. Jung, Woo-Kyun, et al. "Measurement and compensation of spring-back of a hybrid composite beam." *Journal of composite materials* 41.7 (2007): 851-864.
15. Wucher, B., et al. "Tooling geometry optimization for compensation of cure-induced distortions of a curved carbon/epoxy C-spar." *Composites Part A: Applied Science and Manufacturing* 56 (2014): 27-35.